Polymers **2014**, *6*, 1187-1206; doi:10.3390/polym6041187

OPEN ACCESS

polymers

ISSN 2073-4360

www.mdpi.com/journal/polymers

Article

Simplified Modeling of Rectangular Concrete Cross-Sections Confined by External FRP Wrapping

Gian Piero Lignola *, Andrea Prota and Gaetano Manfredi

Department of Structures for Engineering and Architecture, University of Naples "Federico II", Via Claudio 21, Napoli I-80125, Italy; E-Mails: aprota@unina.it (A.P.); gamanfre@unina.it (G.M.)

* Author to whom correspondence should be addressed; E-Mail: glignola@unina.it; Tel.: +39-081-768-3492; Fax: +39-081-768-5921.

Received: 2 December 2013; in revised form: 10 February 2014 / Accepted: 8 April 2014 / Published: 17 April 2014

Abstract: The goal of this research project is to model the effect of confinement by means of fiber reinforced polymer (FRP) externally bonded wrapping, hence to provide a simplified closed form solution to determine directly the ultimate confined concrete strength. Common cross-section shapes for reinforced concrete (RC) columns are considered herein, namely square and rectangular. The simplified model is derived from a more refined iterative confinement model proposed by the same authors to evaluate the entire stress-strain relationship of confined concrete. Based on a detailed analysis of the stress state through Mohr's circle, a simplified closed form solution is proposed to account for the non-uniformly confined concrete performance exhibited in non-axisymmetric sections. The non-uniform confining stress field exhibited in such cross-sections is explicitly considered by means of the mean value integral of the pointwise variable stress state over the cross-section. The key aspect of the proposed methodology is the evaluation of the effective equivalent pressure to be inserted in any triaxial confinement model, to account for the peculiarities of square and rectangular cross-sections. Experimental data, available in the literature and representative of a wide stock of applications, were compared to the results of the theoretical simplified model to validate the proposed approach, and satisfactory results were found.

Keywords: simplified modeling; closed form solution; confined concrete strength; FRP confinement; columns; non-circular cross-sections; externally bonded reinforcement

---

1. Introduction

Within the applications of composites in construction, the confinement of reinforced concrete (RC) columns is one of the most common. Confinement studies date back to early 20th century; however, only in last few decades have extensive experimental and theoretical research documented fiber reinforced polymer (FRP) confinement efficiency (a theoretical background can be found in Di Ludovico *et al.* [1], and a comprehensive updated state-of-the-art on a large amount of confinement tests and models is presented in Ozbakkaloglu *et al.* [2] and Pham and Hadi [3]). For both building columns and bridge piers, the strengthening using FRP strips ensures an easy and fast installation, a strength and/or ductility increase, a high durability, low impact on the use of the structure and almost no increase of mass and geometrical dimensions of the members. Recently, wrapping techniques and materials different from externally bonded strips have been under exam also, like tightly wound glass FRP (GFRP) wires [4] or pre-tensioned propylene ropes [5] without any adhesive.

The confining action of FRP jackets performs better on circular columns, whose geometrical configuration allows the pressure due to fiber wrapping to be uniformly effective on the entire cross-section. The first models proposed at the beginning of last century were based on the Coulomb plasticity criterion (e.g., [6]), so they were based on solid mechanics. It was highlighted that the Coulomb plasticity criterion was very simple, because it proposed a linear relationship between lateral confining pressure, f_l, and confined concrete strength, f_{cc}, both normalized by unconfined concrete strength, f_{co} (Equation (1)), needing the evaluation of a constant, k_1. Solid mechanics-based models have been developed in last few decades, for instance based on triaxial plasticity and calibrated experimentally (e.g., [7]), and they were inserted also into international codes (e.g., [8] in the form of Equation (2)). Solid mechanics-based models have been also proposed [9] to account for the confinement of hollow cross-sections; but due to the non-uniform confining stress field inside the cross-section, they are iterative models. However, to overcome the uncertainty on the definition of sophisticated models, many authors proposed statistically-based models. Regression analyses of the experimental results led to models mainly based on the form reported in Equation (3), where the constants, a and b, are determined according to the best fitting of the experimental data (and sometimes, a and b can be expressed as functions depending also on different parameters).

$$\frac{f_{cc}}{f_{co}} = 1 + k_1 \frac{f_l}{f_{co}} \tag{1}$$

$$\frac{f_{cc}}{f_{co}} = 2.25\sqrt{1 + 7.9\frac{f_l}{f_{co}}} - 2\frac{f_l}{f_{co}} - 1.25 \tag{2}$$

$$\frac{f_{cc}}{f_{co}} = 1 + a\left(\frac{f_l}{f_{co}}\right)^b \tag{3}$$

Whatever the basis of the confinement model, it is crucial to identify uniquely the lateral confining pressure, f_l, to be adopted in the calculation. Most of the models, those that are empirical in nature, have been calibrated against their own sets of experimental data [10].

A more complex behavior characterizes square and rectangular columns; in these cases, due to the presence of the corners, a part of the cross-section remains unconfined, so that square and rectangular

cross-section columns were found to experience less increase in strength and ductility than their circular counterparts. This is because the distribution of lateral confining pressure in circular sections is uniform, in contrast to square and rectangular sections, in which the confining pressure varies from a maximum at the corners along diagonals, to a minimum in between. Similar to the confinement with steel hoops, that loss of effectiveness has been usually "conventionally" modeled with parabolic areas defined by the corners and eventually by longitudinal steel bars. This conventional approach still represents an unresolved issue, even in terms of code provisions. Usually, confinement models proposed in the International Design Codes (e.g., [11–13]) and in the scientific literature for non-circular sections are based on conventional parabolic arching action; parabolic shaped regions are considered, within which the concrete is fully and uniformly confined, while outside the confinement is zero. The evaluation of confining pressure usually is based on an equivalent circular cross-section with diameter D equal to the diagonal of the rectangular cross-section.

2. Theoretical Basis of the Proposed Simplified Approach

Existing analytical models for predicting the behavior of FRP-confined concrete are mostly derived for cylindrical plain concrete columns. Most of the existing models available for non-circular confined concrete assessment both in terms of ultimate capacity and of stress-strain relationships, rely on an assumed value of an "equivalent" lateral confining pressure.

Despite the great research effort in the experimental field, considerable work is still needed to fully outline a definitive analytical model to predict the behavior of FRP confined concrete. A contribution in this direction, to deepen knowledge on non-axisymmetric or non-uniform confinement, is provided by this work.

2.1. Refined Iterative Models

It was originally proposed [14] to adopt Airy's functions to evaluate the in-plane stress field in square concrete cross-sections, under the plane strain assumption (*i.e.*, assuming that the increment of stress due to confinement is produced without any out of plane strain). Starting from that original model, the nonlinear behavior of concrete is accounted for by adopting a secant approach; however, that model provides an "average" confining stress field that is substantially uniform, even in the square, non-circular cross-sections [15].

The authors of [9] proposed a model for hollow cross-sections, where the key innovative aspect of the model is the evaluation of the contribution of a confining stress field not equal in the two transverse directions, x and y (or, in particular, for circular hollow cross-sections, in the radial and circumferential direction). The different and variable contributions were evaluated in each point of the cross-section, explicitly considering a plasticity model for concrete under triaxial compression. However, that model is a refined iterative one, and it required the meshing of the cross-section to evaluate the pointwise performance of concrete confinement.

The transverse stresses (*i.e.*, passive confinement pressure) induced by steel stirrups, either for square or rectangular cross-sections of concrete members axially loaded, are herein evaluated through Airy's functions in a plain strain state assumption, according to the procedure originally proposed for square sections only confined by steel stirrups [14]. The formulation, applying to rectangular

cross-sections and steel stirrups, is finally extended to the case of FRP reinforcement. FRP wrapping is made of elements without flexural stiffness and with a thickness equivalent to the stirrup cross-section over the stirrups' spacing. The proposed model for rectangular cross-sections converges to the confinement of square sections simply considering two equal sides for the cross-section.

2.1.1. Airy's Function $f(x,y)$ for Non-Circular Cross-Section Confinement

The polynomial Airy's function, $f(x,y)$ [14], proposed for rectangular cross-sections is:

$$f(x,y) = -\frac{A_x}{12}x^4 - \frac{B_x L_x^2}{2}x^2 + \frac{C}{2}x^2y^2 - \frac{B_y L_y^2}{2}y^2 - \frac{A_y}{12}y^4 \tag{4}$$

The stresses evaluated according to Equation (5) satisfy equilibrium conditions in the assumption of no mass forces.

$$\sigma_x = \frac{\partial^2 f}{\partial y^2};\ \sigma_y = \frac{\partial^2 f}{\partial x^2};\ \tau_{xy} = \frac{\partial^2 f}{\partial x \partial y} \tag{5}$$

Compatibility is granted by Equation (6), and boundary pressures p_x and p_y are related to the internal stresses, namely σ and τ, through direction cosines, α_x, α_y, of the normal to the sides of the cross-section according to Equation (7).

$$\frac{\partial^4 f}{\partial x^4} + 2\frac{\partial^4 f}{\partial x^2 \partial y^2} + \frac{\partial^4 f}{\partial y^4} = 0 \tag{6}$$

$$\sigma_x \alpha_x + \tau_{yx}\alpha_y = p_x;\ \tau_{xy}\alpha_x + \sigma_y \alpha_y = p_y \tag{7}$$

The unknown parameters to be determined are five, but compatibility condition, Equation (6), reduces the number of unknowns to four, since unknown C must satisfy the relation:

$$A_x + A_y - 2C = 0 \tag{8}$$

The confining stress field inside the cross-section hence is provided by Equation (5):

$$\sigma_x = \frac{A_x + A_y}{2}x^2 - A_y y^2 - B_y L_y^2;\ \sigma_y = \frac{A_x + A_y}{2}y^2 - A_x x^2 - B_x L_x^2;\ \tau_{xy} = -\left(A_x + A_y\right)xy \tag{9}$$

The stress field at the boundaries is depicted in Figure 1, where all the symbols are illustrated.

Figure 1. Boundary stresses and symbols explanation.

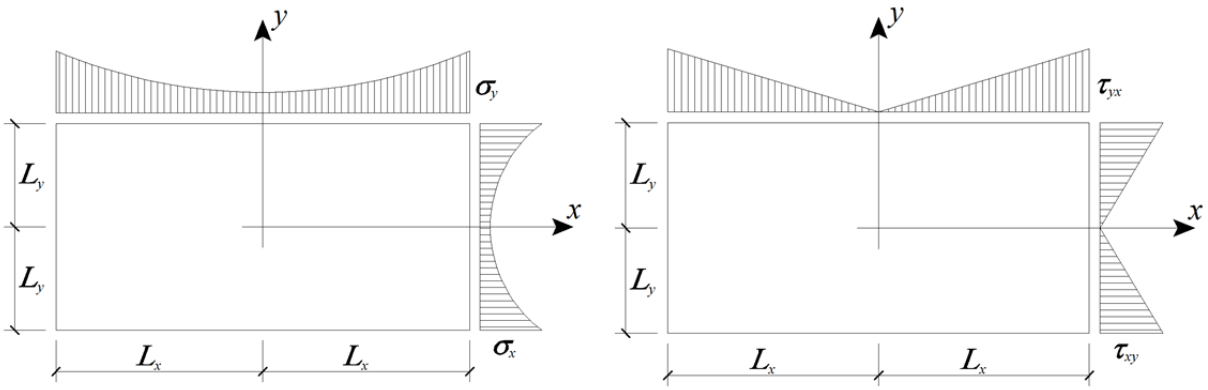

It is assumed that the boundary stresses, *i.e.*, p_x and p_y, are positive if they conform to the local positive axes: in the case of the cross-section depicted in Figure 1, p_x has $\alpha_x = 1$, $\alpha_y = 0$ and $x = L_x$, while p_y has $\alpha_x = 0$, $\alpha_y = 1$ and $y = L_y$, according to Equation (7).

2.1.2. Displacement Compatibility

The four unknown parameters, A_x, A_y, B_x and B_y, have to be determined ensuring displacement compatibility, in the two principal directions, x and y, of the confining device and the concrete sides of the cross-section in both directions perpendicular and parallel to the sides. The compatibility is derived for stirrups (*i.e.*, elements with flexural stiffness, E_fI_s, and axial stiffness, E_fA_s); the cross-section area is equal to A_s, spacing to S and Young's modulus to E_f. The results are simplified in the case of FRP wrapping, where the flexural stiffness, I_s, is negligible (*i.e.*, $I_s = 0$).

The displacements of concrete along x (or y, exchanging x with y) due to confining pressures can be evaluated as:

$$V_{x,c} = \varepsilon_x x + \frac{\gamma_{yx}}{2} y \; ; \; \gamma_{xy} = \frac{2(\nu+1)}{E_c} \tau_{xy} \; ; \; \varepsilon_x = \frac{\sigma_x - \nu\sigma_y}{E_c} \tag{10}$$

The concrete displacement (or deformed shape), in the direction, x, of the side of the cross-section perpendicular to x (*i.e.*, the vertical short side of cross-section depicted in Figure 1), $V_{x,c\perp}$, is obtained from Equation (10) and $x = L_x$. Similarly, the concrete displacement, in the direction, x, of the side of the cross-section parallel to x (*i.e.*, horizontal long side of cross-section depicted in Figure 1), $V_{x,c\parallel}$, is obtained from Equation (10), considering $x = L_x$ and $y = L_y$. These concrete displacements due to confining pressure (concrete contraction) have to be detracted to the expansion along x, $\nu\varepsilon_z L_x$, related to the axial strain, ε_z. Axial strain multiplied by the apparent Poisson ratio (dilation ratio), ν, represents the natural, transverse dilation of the concrete cross-section counteracted by the confining device, yielding to the passive confinement pressure and concrete transverse contraction, $V_{x,c\perp}$ and $V_{x,c\parallel}$.

Each leg of the stirrups can be modeled as a restrained beam: in particular, it has a fixed boundary at the corner, while in the middle section, due to symmetry, it has its rotations restrained, for bending effects, and a fixed boundary, for extensional effects.

The axial displacement in the direction, x, of the leg parallel to x, $V_{x,f\parallel}$, is due to an axial load evaluated by integrating shear stresses, τ_{yx}, acting on that side (*i.e.*, the horizontal long side of the cross-section depicted in Figure 1) and by integrating confining pressures on the leg perpendicular to x of the stirrup:

$$V_{x,f\parallel} = S \frac{A_y + 3B_y}{3E_f A_s} L_x L_y^3 \tag{11}$$

The transverse displacement of the leg perpendicular to x, $V_{x,f\perp}$, is obtained by adding to the displacement, $V_{x,f\parallel}$, the bending displacement of the stirrup (*i.e.*, the vertical short side of the cross-section depicted in Figure 1), in the direction, x, due to the confining pressure, p_x,. In the following expression, E_fI_s is the bending stiffness of the stirrup.

$$V_{x,f\perp}=\frac{A_s\left(L_y^2-y^2\right)^2\left[30B_yL_y^2-15A_xL_x^2+A_y\left(4L_y^2+2y^2-15L_x^2\right)\right]+240\left(A_y+3B_y\right)L_xL_y^3I_s}{720A_sI_sE_f}S \tag{12}$$

2.1.3. Evaluation of Parameters A_x, A_y, B_x and B_y

The least squares method is adopted to evaluate the four unknown coefficients, A_x, A_y, B_x and B_y, of Airy's function. The compatibility in a direction either perpendicular or parallel to each side of the cross-section both along the x and y axes is guaranteed by minimizing the function, g (involving the scatter of the deformed shapes between concrete and stirrups) by setting to zero the derivatives with respect to the four parameters A_x, A_y, B_x and B_y:

$$\begin{aligned}g\left(A_x,A_y,B_x,B_y\right)=&\left(\frac{\int_0^{L_y}\left(\nu\varepsilon_zL_x-V_{x,c\parallel}\right)\mathrm{d}y}{L_y}-\frac{\int_0^{L_y}V_{x,f\parallel}\mathrm{d}y}{L_y}\right)^2+\left(\nu\varepsilon_zL_x-V_{x,c\parallel}-V_{x,f\parallel}\right)^2\\&+\left(\frac{\int_0^{L_x}\left(\nu\varepsilon_zL_y-V_{y,c\perp}\right)\mathrm{d}x}{L_x}-\frac{\int_0^{L_x}V_{y,f\perp}\mathrm{d}x}{L_x}\right)^2+\left(\nu\varepsilon_zL_y-V_{y,c\parallel}-V_{y,f\parallel}\right)^2=\min\end{aligned} \tag{13}$$

$$\left(\frac{\partial g}{\partial A_x}=0\,,\frac{\partial g}{\partial A_y}=0\,,\frac{\partial g}{\partial B_x}=0\,,\frac{\partial g}{\partial B_y}=0\right)\Rightarrow A_x,A_y,B_x,B_y \tag{14}$$

In particular, the perpendicular displacement (e.g., to the x axis) is a function of y; hence, the integral mean value is considered for both concrete and stirrup displacements. The system (14) yields to the values of the relevant parameters. The result, simplified in the case of FRP wrapping (I_s = 0; $t = A_s/S$), is presented for A_x and B_x (and A_y and B_y, exchanging X with Y):

$$A_x=\frac{\nu\left[L_y\left(21L_x^2-21L_xL_y+8L_y^2\right)E_c+6\left(13L_y^2-7L_x^2\right)(1+\nu)E_ft\right]\varepsilon_z}{\frac{4L_x^3L_y^3}{E_ft}\left(\frac{L_x^2}{L_y^2}+\frac{L_y^2}{L_x^2}+\frac{8}{21}\right)E_c+18L_x^2L_y^2\left(L_x+L_y\right)\left(\frac{L_x}{L_y}+\frac{L_y}{L_x}+\frac{91\nu-11}{63}\right)+36L_x^2L_y^2(1+\nu)\left(\frac{L_x^2}{L_y^2}+\frac{L_y^2}{L_x^2}+\frac{20-6\nu}{7}\right)\frac{E_ft}{E_c}} \tag{15}$$

$$B_x=\frac{\frac{\nu\left[L_y\left(21L_y^4-8L_x^2L_y^2+49L_x^3L_y-21L_x^4\right)E_c+6\left(21L_y^4+8L_x^2L_y^2+7L_x^4\right)(1+\nu)E_ft\right]}{L_x^2}\varepsilon_z}{\frac{14L_x^3L_y^3}{E_ft}\left(\frac{L_x^2}{L_y^2}+\frac{L_y^2}{L_x^2}+\frac{8}{21}\right)E_c+63L_x^2L_y^2\left(L_x+L_y\right)\left(\frac{L_x}{L_y}+\frac{L_y}{L_x}+\frac{91\nu-11}{63}\right)+126L_x^2L_y^2(1+\nu)\left(\frac{L_x^2}{L_y^2}+\frac{L_y^2}{L_x^2}+\frac{20-6\nu}{7}\right)\frac{E_ft}{E_c}} \tag{16}$$

2.1.4. The Case of Square Cross-Sections

Furthermore, assuming a square cross-section (*i.e.*, assuming $L_x = L_y = L$, $A_x = A_y = A$ and $B_x = B_y = B$), it is possible to converge to the confinement model for square cross-sections.

The confining stress field inside the cross-section in the case of square cross-sections is given by Equation (9), and it is totally symmetric:

$$\sigma_x = A\left(x^2 - y^2\right) - BL^2;\ \sigma_y = A\left(y^2 - x^2\right) - BL^2;\ \tau_{xy} = -2Axy \tag{17}$$

In this framework, the two parameters, A and B, of Airy's function are rewritten as:

$$A = \frac{21\nu E_c E_f t}{25E_c L^3 + 12E_f tL^2(2\nu + 5)} \cdot \varepsilon_z;\ B = \frac{18\nu E_c E_f t}{25E_c L^3 + 12E_f tL^2(2\nu + 5)} \cdot \varepsilon_z \tag{18}$$

2.2. Simplified Model for Square Sections

Theoretical results, based on the iterative refined model, meshing the cross-section and considering explicitly the pointwise anisotropic confining stress field, have been found [16] to be in satisfactory agreement with the experimental data available in the scientific literature. A previous refined iterative confinement model is herein simplified to account for square sections.

The main goal is to account for the non-uniform confining stress field in the non-circular cross-sections (and different, in different directions), but without explicitly discretizing the cross-section. To avoid the meshing of the section, consequential time consumption and need for software-based approaches, the integral mean is evaluated to provide a closed form solution for this problem. The main idea at the basis of the simplified model is related to the classical Mohr–Coulomb failure envelope theory (Figure 2), according to which, for concrete/soil confined by lateral stress (σ_3), the axial stress (σ_1) is [17]:

$$\sigma_1 = 2c \cdot \tan\left(45° + \frac{\varphi}{2}\right) + \sigma_3 \cdot \tan^2\left(45° + \frac{\varphi}{2}\right) \tag{19}$$

In Equation (19), σ_1 represents the axial strength ($\sigma_1 = f_{cc}$), σ_3 the lateral confining pressure ($\sigma_3 = f_l$), c the cohesion and φ the internal friction angle of the concrete/soil. When $\sigma_3 = 0$, *i.e.*, in the unconfined situation, the unconfined concrete strength (in this case, $\sigma_1 = f_{co}$) can be evaluated removing the lateral confining pressure, hence assuming $\sigma_3 = 0$ in Equation (19), yielding to:

$$f_{co} = 2c \cdot \tan\left(45° + \frac{\varphi}{2}\right) \tag{20}$$

Equation (19) can be rewritten to evaluate directly the confined concrete strength:

$$f_{cc} = f_{co} + f_l \cdot \tan^2\left(45° + \frac{\varphi}{2}\right) = f_{co} + k_1 \cdot f_l \tag{21}$$

The angle of internal friction of concrete varies usually from 36° to 45° [17], and it is not easily estimated from experimental tests. Hence, the angle of internal friction can be assumed as a linear function of concrete strength (Figure 3, where f_{co} is in MPa) as [18]:

$$\varphi = 36° + \left(f_{co}/35\right) \cdot 1° \le 45° \tag{22}$$

Figure 2. Unconfined and confined concrete strength and Mohr–Coulomb failure envelope.

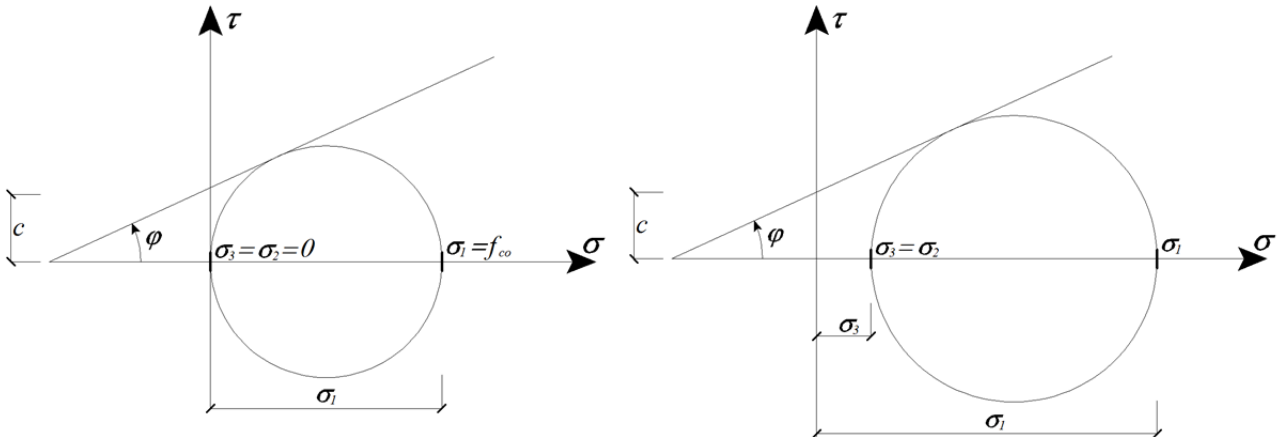

Figure 3. Parameter k_1 of the confinement model: Equations (21) and (22).

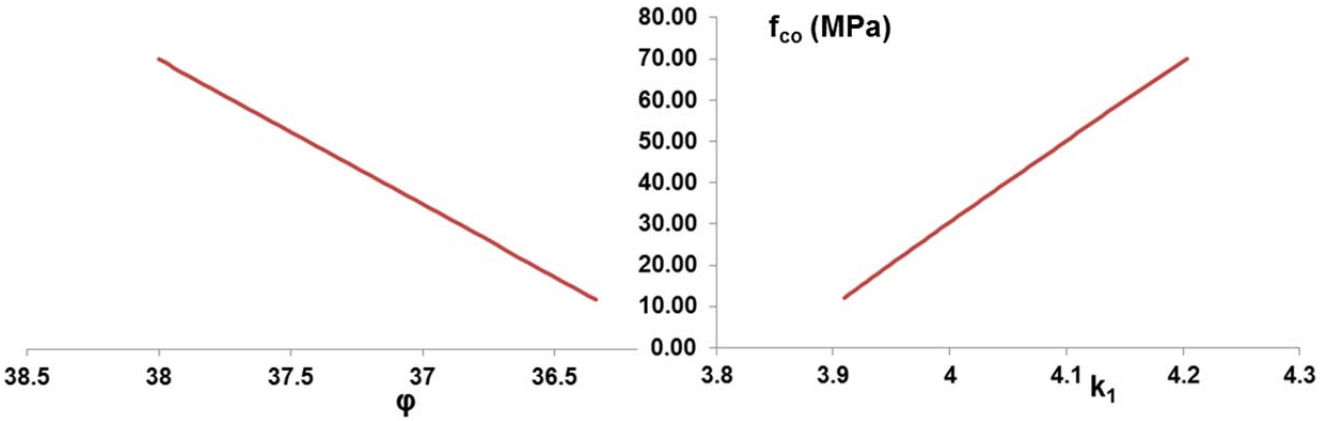

One of the first applications of this theory to confinement was proposed by Richart *et al.* [6] in 1928, and they suggested k_1 = 4.1 corresponding to about φ = 37°, which is an average value for concrete subjected to low confinement pressure. Using triaxial tests, many other authors proposed different expressions for k_1; for instance, k_1 = 3.5 was proposed by Teng *et al.* [19]. Recent studies (e.g., two of the latest are Moran and Pantelides [20] and Girgin [21]) suggested, to best-fit experimental data, that the value of k_1 should be also assumed as a function of the confinement level and should take into account the influence of the concrete strength on the ultimate behavior.

2.2.1. Conventional Procedures to Account for Non-Circular Cross-Sections

In the case of non-circular cross-sections, a shape factor, k_e, is usually defined (Equation (23) as the ratio between the area of "conventional" effectively confined concrete, A_{con}, to the gross sectional area, $A_g = 4L_xL_y$. The effective confined area (Figure 4) is conventionally defined using parabolic arc segments extending between the rounded corners of the section [1].

$$k_e = \frac{A_{con}}{A_g} = 1 - \frac{(L_x - r_c)^2 + (L_y - r_c)^2}{3L_xL_y} \quad (23)$$

Figure 4. Confined and unconfined portion of the section ("conventional" approach). FRP, fiber reinforced polymer.

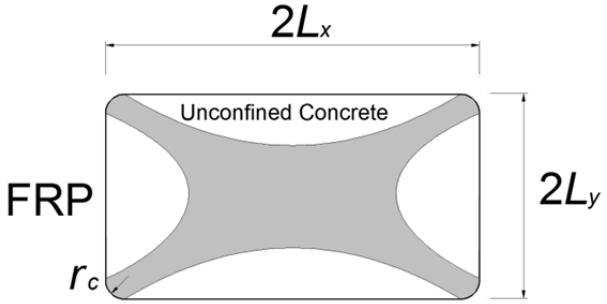

In the case of confinement models based on Equation (1), the shape factor, k_e, can be also adopted to evaluate an "effective" lateral confining pressure. The average strength of a confined concrete column can be evaluated as the axial capacity, N_{cc} (given by the sum of the strength contribution of the confined area, A_{con}, multiplied by f_{cc} and the cover, unconfined, area, A_{cov}, multiplied by f_{co}) divided by the gross area of the section, A_g:

$$\overline{f_{cc}} = \frac{N_{cc}}{A_g} = \frac{\left(f_{co} + k_1 f_l\right) A_{con} + f_{co} A_{cov}}{A_g} = \frac{f_{co}\left(A_{con} + A_{cov}\right) + k_1 f_l A_{con}}{A_g} = f_{co} + k_1 f_l \frac{A_{con}}{A_g} \quad (24)$$

The "effective", or better, the "equivalent", lateral pressure, $k_e f_l$, is the value to be inserted in the confinement model Equation (1) to obtain directly the average strength of the confined concrete in non-circular sections, Equation (24). The main limit of this approach is that the confinement is assumed uniformly constant in between the parabola and zero outside them; furthermore, it is underlined that, even if this procedure was pragmatically extended by many authors and codes (e.g., [11–13]) and also to the models based on nonlinear Equations (2) and (3), the physical meaning of k_e depicted in Equation (24) is not preserved in those cases.

To provide an "effective" lateral pressure, f_l, based on solid mechanics approaches (hence, accounting on the variability of confining pressure over the cross-section) rather than on this "conventional" simplified approach, the following novel procedure is proposed.

2.2.2. Novel Model for "Effective" Confining Pressure

In non-circular applications, the confining pressure is not uniform in the plane of the cross-section (in two perpendicular principal directions, $\sigma_3 = f_{l,min}$ and $\sigma_2 = f_{l,max}$ are different), but in any case, the failure envelope can be related to the minimum confining pressure, σ_3 (Figure 5), the failure circle being independent of σ_2.

Figure 5. Confined concrete strength (related to the Mohr–Coulomb failure envelope theory) under a non-uniform ($\sigma_2 > \sigma_3$) confining pressure field.

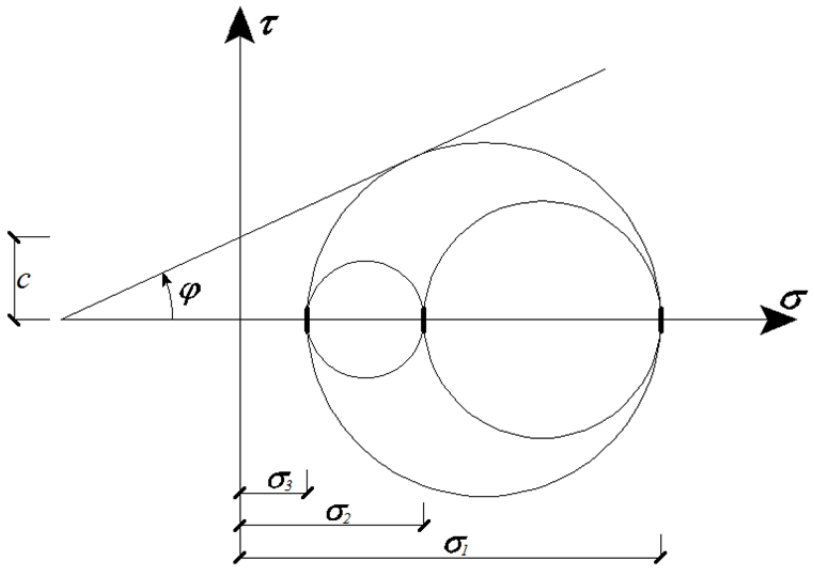

Hence, the strength of concrete is related only to the minimum confining pressure in each point and integrated over the cross-section. The resultant axial force over cross-section Area A_g is evaluated by the integration of pointwise stresses and then divided by the total area, A_g, to provide directly the average confined concrete strength, $f_{cc,sq}$ (see Equation (25)). In this way, an average lateral pressure (the term in brackets in Equation (25)) is evaluated, which can be assumed as the "effective" confining pressure to be inserted in the confinement model to obtain directly, and without any meshing and pointwise evaluation, the confined concrete strength in square sections.

$$f_{cc,sq} = \frac{\int_{\text{Cross-Section}} (f_{cc})\,dA_g}{\int_{\text{Cross-Section}} dA_g} = \frac{\int_{\text{Cross-Section}} (f_{co} + k_1 f_l)\,dA_g}{\int_{\text{Cross-Section}} dA_g} = \\ = f_{co} + k_1 \cdot \left(\frac{\int_{\text{Cross-Section}} (f_{l,min})\,dA_g}{\int_{\text{Cross-Section}} dA_g} \right) = f_{co} + k_1 \cdot f_{l,sq} \quad (25)$$

Given the equation of minimum confining pressure (minimum principal stress), $f_{l,min}$,

$$f_{l,min} = \sigma_3 = \frac{\sigma_x + s_y}{2} - \sqrt{\frac{(\sigma_x - \sigma_y)^2}{4} + \tau_{xy}^2} \quad (26)$$

the closed form solution of $f_{l,sq}$ is given by the solution of integrals in brackets in Equation (25):

$$f_{l,sq} = \frac{4E_c E_f t_f \varepsilon_l}{25E_c L + 12E_f t_f (5 + 2\nu)} \quad (27)$$

In Equation (27) many parameters appear: L is the half length of a side of the square cross-section; E_f and t_f are, respectively, the Young's modulus and total thickness of the wrap; ε_l is the strain in the wrap; and finally, the nonlinear mechanical properties of concrete are (secant) Young's modulus E_c

and apparent Poisson ratio (dilation ratio) ν at failure. However, it can be easily verified that for typical values of involved parameters, the numerical influence of ν (even ranging widely between zero and two) is negligible in Equation (27); hence, to simplify the evaluation, ν can be approximately fixed equal to 0.5. This simplifies the calculation, while more refined evaluations can be based on the iterative evaluation of $\nu = \varepsilon_l/\varepsilon_{cc}$. Conversely, E_c has a major impact, and it can be evaluated iteratively as the ratio between f_{cc} (evaluated according to Equation (25)) and ultimate concrete strain, ε_{cc}, which can be assumed [6] equal to:

$$\varepsilon_{cc} = \varepsilon_{co}\left(5\frac{f_{cc}}{f_{co}} - 4\right) \tag{28}$$

In the previous equation, ε_{cc} is the concrete strain corresponding to f_{cc}, and convergence on E_c can be found via a spreadsheet with very few iterations, starting with a trial value equal to the elastic tangent, E_c. In this procedure, the evaluation of ultimate concrete strain plays a crucial role to account for concrete nonlinearities (ν and E_c); hence, it will be the focus of future developments and improvements of the predictability of the model. The procedure is based on the evaluation of $f_{cc,sq}$ (according to Equation (25)), where $f_{l,sq}$ is evaluated based on trial E_c (according to Equation (27)); this value of $f_{cc,sq}$ is divided by ε_{cc} (according to Equation (28)), providing the new value of E_c which converges to the previous trial E_c in very few iterations. It is noted that Equation (25) is the core of the methodology, it being possible to insert every confinement model to calculate f_{cc}. However, the resulting integral does not always have a simple closed form solution, as in the case of the linear model, Equation (21), adopted in this study (which is based on the Mohr–Coulomb failure envelope theory).

3. Proposed Simplified Confinement Model for Rectangular Sections

3.1. Implementation of the Model

Theoretically, the direct integration of Equation (25) for rectangular cross-sections (with stresses evaluated according to Equation (9) based on coefficients A_x, A_y, B_x and B_y, provided by Equations (15) and (16)) is feasible, and it provides results for rectangular cross-sections, as well. However, it does not provide simple closed form solutions, and it can be solved numerically via computer algebra software (CAS). Because the aim of this paper is to provide a direct, practical tool, oriented toward the profession, a further simplification was conceived of to model confinement for rectangular cross-sections.

The basic idea is that a rectangular cross-section can be assumed as in between two square sections, for which a simplified, yet reliable, confinement model has been just provided. A rectangular section having side aspect ratio $\zeta = L_x/L_y = 1$ is a square section, so that the confined concrete strength should be equal to $f_{cc,sq}$; on the other hand, a rectangular section having side aspect ratio $\zeta \geq 3$ is a slender wall-like cross-section, so that the confined concrete strength should be evaluated according to another specific model proposed by the authors for such a cross-section shape [22]. Finally a cross-section having $1 < \zeta < 3$ is expected to be in between the two limit cases, and it is the suggested range of applicability for this model. In view of this basic idea, the behavior of a rectangular cross-section is assumed as in between the behavior of two square cross-sections having the sides equal to the longest

($2L_x$) and the shortest ($2L_y$) sides of the rectangular cross-section. In this procedure, the adopted confinement equation, Equation (21), is linear; hence, the average of $f_{cc,sq}$ for the two considered "limit" square cross-sections yields to the average of the lateral confining stresses:

$$f_{cc,rect} = \frac{f_{cc,sq}(L_x) + f_{cc,sq}(L_y)}{2} = f_{co} + k_1 \cdot \frac{f_{l,sq}(L_x) + f_{l,sq}(L_y)}{2} = f_{co} + k_1 \cdot f_{l,rect} \quad (29)$$

$$f_{l,rect} = \left(\frac{2E_c E_f t_f}{25E_c L_x + 12E_f t_f (5+2\nu)} + \frac{2E_c E_f t_f}{25E_c L_y + 12E_f t_f (5+2\nu)} \right) \varepsilon_l \quad (30)$$

An outline of the proposed model is depicted in Figure 6. Similarly to the case of square cross-sections, the nonlinear parameter, E_c, can be found with very few iterations (as discussed in Section 2.2.2), and the influence of ν is again negligible, as will be discussed during the experimental validation of the model.

Figure 6. Outline of the proposed simplified confinement model.

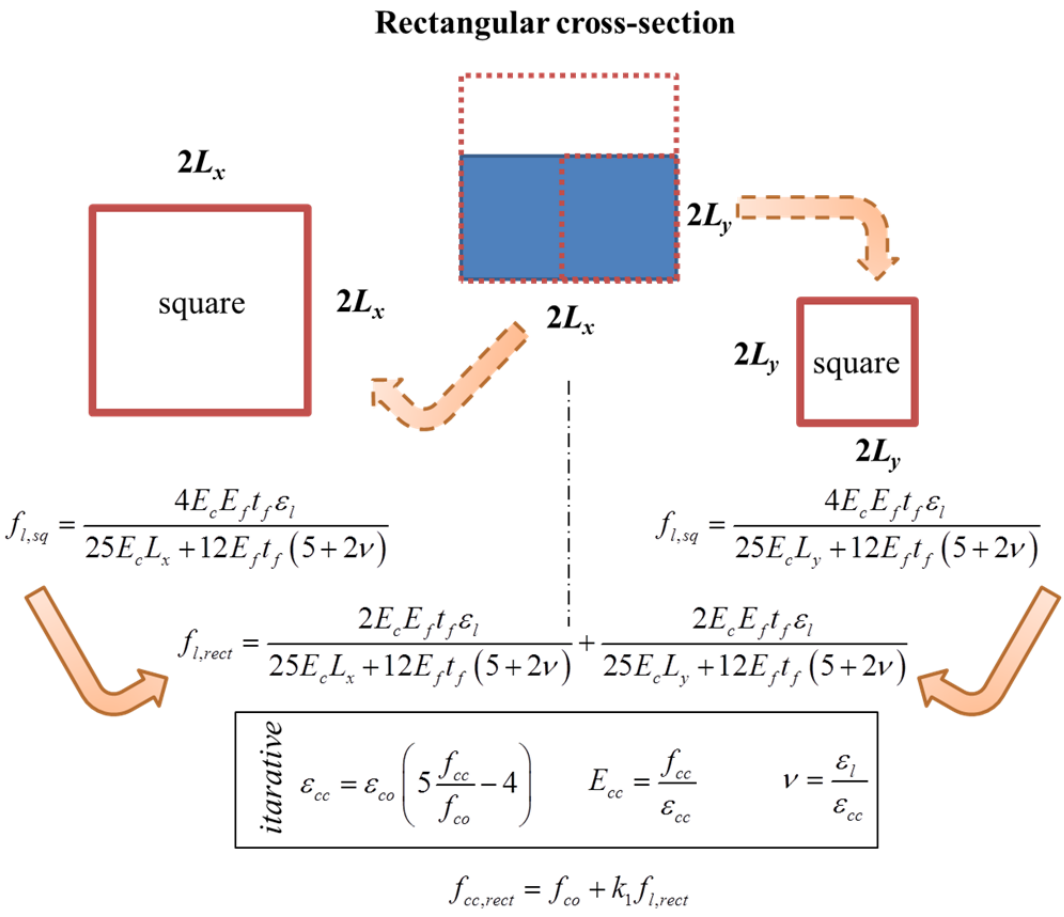

3.2. Validation of the Model

The proposed confinement model has been validated by means of experimental theoretical comparisons based on an experimental database [23–41] involving 136 square columns and 44 rectangular columns. The minimum and maximum dimensions of the cross-sections in the database are 150 and 1270 mm, always with $\zeta \leq 2$; the concrete unconfined strength ranges between 12 and 54.1 MPa. Different fiber types for wraps were used with a total thickness ranging between 0.047 and 9.6 mm and an elastic modulus ranging between five and 355 GPa. In this sense, the database is representative of a wide stock. The validation is summarized in the following Tables 1 and 2 and in Figure 7, dividing, in the well-known format of the 45° line, square sections from rectangular sections. Common synthetic indexes showing the reliability of the confinement model (e.g., [2]) are the average, μ, of the ratios of confined concrete strength (theoretical $f_{cc,sq}$ or $f_{cc,rect}$ over experimental $f_{cc,EXP}$) and their coefficient of variation (*CV*). It results that μ is equal to 0.90 and 0.97, while *CV* is equal to 13% and 12%, respectively, for square and rectangular cross-sections, with the approximated constant ν value assumed equal to 0.5. The average, μ, focuses on overall model accuracy, and it is noted that ratios lower than one represent safe side predictions, because the prediction is lower than the actual experimental value. Similarly, *CV* shows the magnitude of the associated variability to the mean error.

Figure 7. Validation of the proposed model (experimental *vs.* theoretical strength; 45° line).

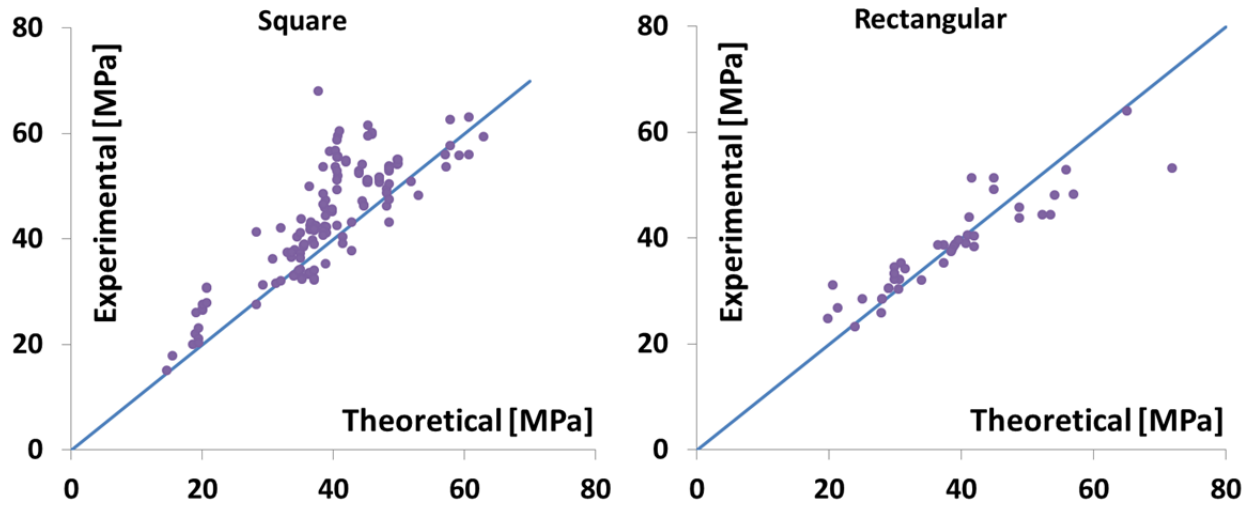

Implementing an iterative procedure also to determine *v* as the ratio between lateral and axial strain, $\nu = \varepsilon_l/\varepsilon_{cc}$, μ results in being equal to 0.92 and 0.97, while *CV* is equal to 13% and 12%, respectively, for square and rectangular cross-sections. It is clear that the improvement in terms of predictions is not relevant compared to the added complexity of the model.

Table 1. Experimental theoretical comparison: square cross-sections.

Ref.	f_{co} (MPa)	$2L$ (mm)	Fiber	t_f (mm)	E_f (GPa)	ε_l (%)	$f_{cc,EXP}$ (MPa)	$f_{l,sq}$ (MPa)	$f_{cc,sq}$ (MPa)	THEOR. / EXP.
Campione (2006) [23]	12.0	150	CFRP	0.165	230.0	1.50	15.1	0.84	15.27	1.01
	12.0	150	CFRP	0.330	230.0	1.50	17.8	1.20	16.67	0.94
Rousakis *et al.* (2007) [24]	33.0	200	CFRP	0.117	240.0	1.55	38.4	0.66	35.69	0.93
	33.0	200	CFRP	0.117	240.0	1.55	38.8	0.66	35.69	0.92
	33.0	200	CFRP	0.351	240.0	1.55	45.9	1.72	39.94	0.87
	33.0	200	CFRP	0.351	240.0	1.55	42.4	1.72	39.94	0.94
	33.0	200	CFRP	0.585	240.0	1.55	55.6	2.48	42.98	0.77
	33.0	200	CFRP	0.585	240.0	1.55	59.5	2.48	42.98	0.72
	33.0	200	GFRP	0.351	65.0	2.80	42.6	0.97	36.94	0.87
	33.0	200	GFRP	0.351	65.0	2.80	41.8	0.97	36.94	0.88
	33.0	200	GFRP	0.702	65.0	2.80	44.4	1.83	40.37	0.91
	33.0	200	GFRP	0.702	65.0	2.80	47.3	1.83	40.37	0.85
	33.0	200	GFRP	1.053	65.0	2.80	51.9	2.56	43.29	0.83
	33.0	200	GFRP	1.053	65.0	2.80	55.5	2.56	43.29	0.78
	34.2	200	CFRP	0.117	240.0	1.55	42.2	0.66	36.84	0.87
	34.2	200	CFRP	0.117	240.0	1.55	41.9	0.66	36.84	0.88
	34.2	200	CFRP	0.351	240.0	1.55	45.2	1.71	41.07	0.91
	34.2	200	CFRP	0.351	240.0	1.55	45.7	1.71	41.07	0.90
	34.2	200	CFRP	0.585	240.0	1.55	54.6	2.46	44.06	0.81
	34.2	200	CFRP	0.585	240.0	1.55	54.9	2.46	44.06	0.80
	38.0	200	GFRP	0.351	65.0	2.80	40.4	0.97	41.88	1.04
	38.0	200	GFRP	0.351	65.0	2.80	39.1	0.97	41.88	1.07
	38.0	200	GFRP	0.702	65.0	2.80	52.8	1.81	45.28	0.86
	38.0	200	GFRP	0.702	65.0	2.80	52.4	1.81	45.28	0.86
	38.0	200	GFRP	1.053	65.0	2.80	59.8	2.52	48.14	0.81
	38.0	200	GFRP	1.053	65.0	2.80	60.2	2.52	48.14	0.80
	39.9	200	GFRP	0.351	65.0	2.80	43.1	0.78	43.06	1.00
	39.9	200	GFRP	0.351	65.0	2.80	37.7	0.78	43.06	1.14
	39.9	200	GFRP	0.702	65.0	2.80	54.2	1.21	44.79	0.83
	39.9	200	GFRP	0.702	65.0	2.80	47.1	1.21	44.79	0.95
	39.9	200	GFRP	1.053	65.0	2.80	59.5	1.46	45.82	0.77
	39.9	200	GFRP	1.053	65.0	2.80	61.5	1.46	45.82	0.74
Wang and Wu (2008) [25]	31.7	150	CFRP	0.165	219.0	1.99	33.2	1.35	37.09	1.12
	31.7	150	CFRP	0.330	219.0	1.99	35.2	2.30	40.90	1.16
	52.1	150	CFRP	0.165	225.7	1.92	53.7	1.42	57.91	1.08
	52.1	150	CFRP	0.330	225.7	1.92	55.9	2.58	62.67	1.12
	31.9	150	CFRP	0.165	219.0	1.99	33.6	1.35	37.29	1.11
	31.9	150	CFRP	0.330	219.0	1.99	42.2	2.31	41.12	0.97
	54.1	150	CFRP	0.165	225.7	1.92	55.8	1.42	59.94	1.07
	54.1	150	CFRP	0.330	225.7	1.92	59.4	2.60	64.77	1.09

Table 1. *Cont.*

Ref.	f_{co} (MPa)	$2L$ (mm)	Fiber	t_f (mm)	E_f (GPa)	ε_l (%)	$f_{cc,EXP}$ (MPa)	$f_{l,sq}$ (MPa)	$f_{cc,sq}$ (MPa)	THEOR. / EXP.
Wang and Wu (2008) [25]	32.3	150	CFRP	0.165	219.0	1.99	39.8	1.35	37.71	0.95
	32.3	150	CFRP	0.330	219.0	1.99	56.5	2.32	41.56	0.74
	52.0	150	CFRP	0.165	225.7	1.92	55.9	1.42	57.81	1.03
	52.0	150	CFRP	0.330	225.7	1.92	63.0	2.58	62.56	0.99
	30.7	150	CFRP	0.165	219.0	1.99	43.7	1.34	36.05	0.83
	30.7	150	CFRP	0.330	219.0	1.99	68.0	2.28	39.80	0.59
	52.7	150	CFRP	0.165	225.7	1.92	57.6	1.42	58.52	1.02
	52.7	150	CFRP	0.330	225.7	1.92	80.3	2.58	63.30	0.79
	31.8	150	CFRP	0.165	219.0	1.99	50.0	1.35	37.19	0.74
	52.7	150	CFRP	0.165	225.7	1.92	62.6	1.42	58.52	0.93
	52.7	150	CFRP	0.330	225.7	1.92	89.8	2.58	63.30	0.70
Harries and Carey (2003) [26]	32.4	152	GFRP	3.000	4.9	1.60	37.9	0.47	34.28	0.90
	32.4	152	GFRP	9.000	4.9	1.60	43.2	1.23	37.30	0.86
	31.2	152	GFRP	3.000	4.9	1.60	37.4	0.48	33.11	0.89
	31.2	152	GFRP	9.000	4.9	1.60	39.0	1.31	36.43	0.93
Shehata *et al.* (2002) [27]	23.7	150	CFRP	0.165	355.0	1.50	27.5	1.47	29.53	1.07
	29.5	150	CFRP	0.165	355.0	1.50	40.4	1.55	35.69	0.88
Lam *et al.* (2006) [28]	35.3	150	CFRP	0.167	230.0	1.50	41.2	1.02	39.39	0.96
	35.3	150	CFRP	0.334	230.0	1.50	60.4	1.66	41.98	0.69
Ilki and Kumbasar (2003) [29]	32.8	250	CFRP	0.165	230.0	1.50	32.7	0.68	35.53	1.09
	32.8	250	CFRP	0.165	230.0	1.50	32.3	0.68	35.53	1.10
	32.8	250	CFRP	0.495	230.0	1.50	41.4	1.72	39.69	0.96
	32.8	250	CFRP	0.495	230.0	1.50	40.6	1.72	39.69	0.98
	32.8	250	CFRP	0.825	230.0	1.50	56.7	2.41	42.46	0.75
	32.8	250	CFRP	0.825	230.0	1.50	53.6	2.41	42.46	0.79
Al-Salloum (2006) [30]	28.7	150	CFRP	1.200	75.1	1.50	41.2	1.99	36.62	0.89
	30.9	150	CFRP	1.200	75.1	1.50	42.5	2.04	39.06	0.92
Harajli (2006) [31]	42.0	152	CFRP	0.900	82.0	1.50	49.5	1.77	49.17	0.99
	42.0	152	CFRP	0.900	82.0	1.50	46.2	1.77	49.17	1.06
	42.0	152	CFRP	0.900	82.0	1.50	48.7	1.77	49.17	1.01
Masia *et al.* (2004) [32]	26.3	152	GFRP	1.000	19.1	2.40	31.3	0.89	29.83	0.95
	26.3	152	GFRP	2.000	19.1	2.40	31.6	1.60	32.66	1.03
	26.3	152	GFRP	1.000	19.1	1.50	41.3	0.56	28.53	0.69
Mandal *et al.* (2005) [33]	31.5	458	GFRP	3.000	19.1	1.50	36.5	0.56	33.76	0.92
	31.5	458	GFRP	3.000	19.1	1.50	37.5	0.56	33.76	0.90
	31.9	152	GFRP	3.000	10.3	1.50	37.3	0.88	35.41	0.95
	31.9	152	GFRP	3.000	10.3	1.50	36.4	0.88	35.41	0.97
	31.9	152	GFRP	3.000	10.3	1.50	34.1	0.88	35.41	1.04
	31.9	152	GFRP	9.000	10.3	1.50	53.6	2.03	40.03	0.75
	31.9	152	GFRP	9.000	10.3	1.50	46.6	2.03	40.03	0.86
	31.9	152	GFRP	9.000	10.3	1.50	48.5	2.03	40.03	0.83
Wang and Wu (2008) [25]	15.0	279	GFRP	2.000	87.0	1.40	26.0	1.35	20.27	0.78
	15.0	279	GFRP	9.600	17.0	1.40	22.0	1.31	20.14	0.92
Tao *et al.* (2008) [34]	43.0	152	GFRP	1.260	13.6	1.69	50.7	0.59	45.38	0.89
	43.0	152	GFRP	2.520	13.6	1.69	51.6	1.12	47.53	0.92
	43.0	152	GFRP	3.780	13.6	1.69	53.8	1.59	49.44	0.92

Table 1. *Cont.*

Ref.	f_{co} (MPa)	$2L$ (mm)	Fiber	t_f (mm)	E_f (GPa)	ε_l (%)	$f_{cc,EXP}$ (MPa)	$f_{l,sq}$ (MPa)	$f_{cc,sq}$ (MPa)	THEOR. / EXP.
Tao *et al.* (2008) [34]	43.0	152	GFRP	5.040	13.6	1.69	54.2	2.00	51.12	0.94
	43.0	152	GFRP	1.260	13.6	1.69	51.2	0.59	45.38	0.89
	43.0	152	GFRP	2.520	13.6	1.69	51.2	1.12	47.53	0.93
	43.0	152	GFRP	3.780	13.6	1.69	53.3	1.59	49.44	0.93
	43.0	152	GFRP	5.040	13.6	1.69	55.0	2.00	51.12	0.93
	43.0	152	GFRP	2.520	13.6	1.69	50.7	1.12	47.53	0.94
	43.0	152	GFRP	3.780	13.6	1.69	52.9	1.59	49.44	0.93
Micelli and Modarelli (2013) [35]	28.0	150	CFRP	0.330	221.0	1.40	32.0	1.13	32.50	1.02
	28.0	150	CFRP	0.165	221.0	1.40	36.2	0.77	31.06	0.86
	28.0	150	CFRP	0.330	221.0	1.40	42.1	1.13	32.50	0.77
Faella *et al.* (2004) [36]	30.0	150	GFRP	0.480	80.7	3.50	32.1	2.42	39.65	1.23
	30.0	150	GFRP	0.480	80.7	3.50	32.5	2.42	39.65	1.22
	30.0	150	GFRP	0.480	80.7	3.50	41.5	2.42	39.65	0.95
	30.0	150	GFRP	0.480	80.7	3.50	34.1	2.42	39.65	1.16
	30.0	150	GFRP	0.480	80.7	3.50	41.9	2.42	39.65	0.95
	30.0	150	GFRP	0.480	80.7	3.50	38.9	2.42	39.65	1.02
	30.0	150	GFRP	0.960	80.7	3.50	42.5	3.93	45.69	1.07
	30.0	150	GFRP	0.960	80.7	3.50	49.3	3.93	45.69	0.93
	30.0	150	GFRP	0.960	80.7	3.50	51.2	3.93	45.69	0.89
	30.0	150	GFRP	0.960	80.7	3.50	52.9	3.93	45.69	0.86
	30.0	150	GFRP	0.960	80.7	3.50	58.7	3.93	45.69	0.78
	30.0	150	GFRP	0.960	80.7	3.50	55.5	3.93	45.69	0.82
Ombres (2006) [37]	17.4	150	CFRP	0.047	240.0	1.42	20.0	0.32	18.68	0.93
	17.4	150	CFRP	0.094	240.0	1.42	23.1	0.60	19.76	0.85
	17.4	150	CFRP	0.094	240.0	1.42	21.1	0.60	19.76	0.94
	17.4	150	CFRP	0.094	240.0	1.42	20.2	0.60	19.76	0.98
	17.4	150	CFRP	0.141	240.0	1.42	26.4	0.82	20.66	0.78
	17.4	150	CFRP	0.141	240.0	1.42	26.8	0.82	20.66	0.77
	17.4	150	CFRP	0.141	240.0	1.42	27.5	0.82	20.66	0.75
	17.4	150	CFRP	0.188	240.0	1.42	30.6	1.01	21.40	0.70
	17.4	150	CFRP	0.188	240.0	1.42	27.9	1.01	21.40	0.77
	17.4	150	CFRP	0.188	240.0	1.42	30.7	1.01	21.40	0.70
Demers and Neale (1999) [38]	32.3	152	GFRP	1.050	10.5	2.00	33.1	0.45	34.10	1.03
	32.3	152	GFRP	1.050	10.5	2.00	33.0	0.45	34.10	1.03
	32.3	152	CFRP	0.900	25.0	1.50	34.1	0.66	34.96	1.03
	42.2	152	CFRP	0.900	25.0	1.50	46.4	0.68	44.94	0.97
	42.2	152	CFRP	0.900	25.0	1.50	46.3	0.68	44.94	0.97
Rochette and Labossiere (2000) [39]	42.0	152	CFRP	0.900	82.7	1.50	43.2	1.93	49.81	1.15
	42.0	152	CFRP	0.900	82.7	1.50	47.4	1.93	49.81	1.05
	42.0	152	CFRP	0.900	82.7	1.50	50.4	1.93	49.81	0.99
	43.9	152	CFRP	1.500	82.7	1.50	48.3	2.82	55.33	1.15
	43.9	152	CFRP	1.200	82.7	1.50	50.9	2.42	53.71	1.06
	43.0	152	AFRP	1.260	13.6	1.70	50.7	0.59	45.40	0.90
	43.0	152	AFRP	2.520	13.6	1.70	51.6	1.13	47.59	0.92
	43.0	152	AFRP	3.780	13.6	1.70	53.7	1.62	49.55	0.92
	43.0	152	AFRP	5.040	13.6	1.70	54.2	2.05	51.30	0.95
	43.0	152	AFRP	1.260	13.6	1.70	51.2	0.59	45.40	0.89

Table 2. Experimental theoretical comparison: Rectangular cross-sections.

Ref.	f_{co} (MPa)	$2L_x$ (mm)	$2L_y$ (mm)	Fiber	t_f (mm)	E_f (GPa)	ε_l (%)	$f_{cc,EXP}$ (MPa)	$f_{l,rect}$ (MPa)	$f_{cc,rect}$ (MPa)	THEOR. / EXP.
Lam *et al.* (2006) [28]	35.3	188	150	CFRP	0.334	230.0	1.50	51.4	1.55	41.53	0.81
	35.3	225	150	CFRP	0.334	230.0	1.50	43.9	1.47	41.20	0.94
	35.3	263	150	CFRP	0.334	230.0	1.50	40.5	1.40	40.93	1.01
	35.3	300	150	CFRP	0.334	230.0	1.50	39.0	1.35	40.72	1.04
	35.3	188	150	CFRP	0.167	230.0	1.50	38.8	0.93	39.05	1.01
	35.3	225	150	CFRP	0.167	230.0	1.50	38.4	0.87	38.81	1.01
	35.3	263	150	CFRP	0.167	230.0	1.50	37.7	0.83	38.63	1.02
	35.3	300	150	CFRP	0.167	230.0	1.50	37.4	0.79	38.49	1.03
Ilki and Kumbasar (2003) [29]	34.0	300	150	CFRP	0.165	230.0	1.50	35.2	0.83	37.33	1.06
	34.0	300	150	CFRP	0.165	230.0	1.50	38.7	0.83	37.33	0.96
	34.0	300	150	CFRP	0.495	230.0	1.50	40.4	2.00	42.00	1.04
	34.0	300	150	CFRP	0.495	230.0	1.50	38.4	2.00	42.00	1.09
	34.0	300	150	CFRP	0.825	230.0	1.50	49.2	2.71	44.88	0.91
	34.0	300	150	CFRP	0.825	230.0	1.50	51.3	2.71	44.88	0.87
Rochette and Laboissiere (2000) [39]	42.0	203	152	GFRP	0.900	86.0	1.50	45.8	1.66	48.72	1.06
	42.0	203	152	GFRP	0.900	86.0	1.50	43.7	1.66	48.72	1.11
	43.9	203	152	GFRP	1.500	86.0	1.50	44.3	2.36	53.49	1.21
	43.9	203	152	GFRP	1.200	86.0	1.50	44.4	2.05	52.23	1.18
Demers and Neale (1999) [38]	17.6	200	150	CFRP	0.165	221.0	1.40	24.8	0.56	19.79	0.80
	17.6	200	150	CFRP	0.330	221.0	1.40	31.2	0.75	20.54	0.66
	17.6	200	150	GFRP	0.460	86.0	2.30	26.8	0.95	21.35	0.80
Chaallal *et al.* (2003) [40]	37.7	354	250	GFRP	0.600	60.0	1.30	39.6	0.47	39.61	1.00
	22.8	635	318	CFRP	0.167	280.0	0.90	23.3	0.30	23.97	1.03
	22.8	635	318	CFRP	0.334	280.0	0.90	28.5	0.57	25.03	0.88
	24.1	1270	635	CFRP	3.173	280.0	0.90	35.2	1.72	30.92	0.88
Parving and Wang (2001) [41]	46.4	510	360	GFRP	1.160	72.0	4.50	48.3	2.59	56.94	1.18
	49.7	510	360	GFRP	2.900	72.0	4.50	53.2	5.42	71.86	1.35
	53.8	510	360	GFRP	1.200	77.0	4.40	64.0	2.73	65.01	1.02
	46.8	510	360	GFRP	0.960	80.0	4.20	52.9	2.23	55.90	1.06
	47.6	740	510	GFRP	0.960	80.0	4.20	48.1	1.60	54.11	1.13
Micelli and Modarelli (2013) [35]	28.0	200	150	CFRP	0.165	221.0	1.40	30.3	0.63	30.50	1.01
	28.0	200	150	CFRP	0.330	221.0	1.40	34.1	0.90	31.56	0.93
	28.0	200	150	GFRP	0.230	85.0	2.28	32.2	0.65	30.59	0.95
Ombres (2006) [37]	27.1	300	150	CFRP	0.047	240.0	1.42	28.5	0.25	28.05	0.98
	27.1	300	150	CFRP	0.047	240.0	1.42	28.5	0.25	28.05	0.98
	27.1	300	150	CFRP	0.094	240.0	1.42	30.5	0.49	29.00	0.95
	27.1	300	150	CFRP	0.094	240.0	1.42	30.5	0.49	29.00	0.95
	27.1	300	150	CFRP	0.141	240.0	1.42	34.4	0.72	29.90	0.87
	27.1	300	150	CFRP	0.141	240.0	1.42	33.3	0.72	29.90	0.90
	27.1	300	150	CFRP	0.141	240.0	1.42	32.2	0.72	29.90	0.93
Shehata *et al.* (2002) [27]	23.7	188	94	CFRP	0.165	235.0	1.50	25.8	1.07	27.92	1.08
	23.7	188	94	CFRP	0.330	235.0	1.50	33.2	1.58	29.95	0.90
	29.5	188	94	CFRP	0.165	235.0	1.50	32.0	1.14	34.05	1.06
	29.5	188	94	CFRP	0.330	235.0	1.50	38.7	1.76	36.52	0.94

4. Conclusions

The proposed simplified model was derived from a more refined iterative confinement model previously proposed by the same authors. This represents an attempt to account for the pointwise variability of the confinement stress field over the cross-section, but keeping a simplified calculation, without meshing the cross-section. Hence, an "effective" confining pressure was provided to obtain directly the confined concrete strength in square sections. In any case, the model accounts explicitly for the non-uniform confined concrete performance pointwise exhibited in non-axisymmetric sections by means of the integral mean of stresses over the cross-section. However, the integration method discussed in the paper provides also refined solutions for rectangular cross-sections; a simple closed form solution cannot be provided, but CAS software only provides the numerical solution to the problem. To preserve the scope of providing simplified equations, a further assumption was introduced in the case of rectangular cross-sections: they are considered as in between the behavior of two "limit" square cross-sections, having sides equal to the shortest and longest sides of the rectangular cross-section.

To account for concrete nonlinearity close to failure, the model is still iterative (but very few iterations provide converge); in any case, the iterations can be simply implemented in a spreadsheet. Future development will include the improvement of concrete ultimate strain evaluations related to the nonlinearities.

To validate the proposed approach, experimental data, representative of a wide stock of common typical confinement applications, available in the literature, were compared to the predictions of the theoretical simplified analysis, and satisfactory agreement was achieved. The simplified model gives rather accurate results despite the heavily reduced computational effort, if compared to the refined iterative algorithm previously proposed by the same authors.

Acknowledgments

The analyses were developed within the activities of Rete dei Laboratori Universitari di Ingegneria Sismica (ReLUIS) for the research program funded by the Dipartimento di Protezione Civile, Progetto Esecutivo 2010–2013.

Conflicts of Interest

The authors declare no conflict of interest.

References

1. Di Ludovico, M.; Ceroni, F.; Lignola, G.P.; Prota, A.; Manfredi, G.; Cosenza, E. *Externally Bonded Reinforced Concrete Structures*; Wiley Encyclopedia of Composites, John Wiley & Sons, Inc.: Chichester, UK, 2012; pp. 1–17.
2. Ozbakkaloglu, T.; Lim, J.C.; Vincent, T. FRP-confined concrete in circular sections: Review and assessment of stress–strain models. *Eng. Struct.* **2013**, *49*, 1068–1088.
3. Pham, T.; Hadi, M. Stress prediction model for FRP confined rectangular concrete columns with rounded corners. *J. Compos. Constr.* **2014**, doi:10.1061/(ASCE)CC.1943-5614.0000407.
4. Choi, E.; Jeon, J.; Cho, B.; Park, K. External jacket of FRP wire for confining concrete and its advantages. *Eng. Struct.* **2013**, *56*, 555–566.

5. Rousakis, T.C.; Tourtouras, I.S. RC columns of square section—Passive and active confinement with composite ropes. *Compos. B Eng.* **2014**, *58*, 573–581.
6. Richart, F.E.; Brandtzaeg, A.; .Brown, R.L. *A Study of the Failure of Concrete under Combined Compressive Stresses*; University of Illinois Engineering Experimental Station: Champaign, IL, USA, 1928; Bulletin No. 185, Volume XXVI, No. 12.
7. Elwi, A.A.; Murray, D.W. A 3D hypoelastic concrete constitutive relationship. *J. Eng. Mech. Div.* **1979**, *105*, 623–641.
8. American Concrete Institute. *Guide for the Design and Construction of Externally Bonded FRP Systems for Strengthening of Concrete Structure*; ACI 440.2R-02; American Concrete Institute: Farmington Hill, MI, USA, 2002.
9. Lignola, G.P.; Prota, A.; Manfredi, G.; Cosenza, E. Unified theory for confinement of RC solid and hollow circular columns. *Compos. B Eng.* **2008**, *39*, 1151–1160.
10. De Lorenzis, L.; Tepfers, R. Comparative study of models on confinement of concrete cylinders with fiber reinforced polymer composites. *J. Compos. Constr.* **2003**, 7, 219–237.
11. American Concrete Institute. *Guide for the Design and Construction of Externally Bonded FRP Systems for Strengthening of Concrete Structure*; ACI 440.2R-08; American Concrete Institute: Farmington Hill, MI, USA, 2008.
12. CEN European Standard EN 1998-3. *Eurocode 8: Design of Structures for Earthquake Resistance—Part 3: Assessment and Retrofitting of Buildings*; European Committee for Standardization: Brussels, Belgium, 2005.
13. CNR-DT 200 R1. *Guide for the Design and Construction of Externally Bonded FRP Systems for Strengthening Existing Structures*; National Research Council: Rome, Italy, 2013.
14. Braga, F.; Gigliotti, R.; Laterza, M. Analytical stress–strain relationship for concrete confined by steel stirrups and/or FRP jackets. *J. Struct. Eng.* **2006**, *132*, 1402–1416.
15. D'Amato, M.; Braga, F.; Gigliotti, R.; Kunnath, S.; Laterza, M. A numerical general-purpose confinement model for non-linear analysis of R/C members. *Comput. Struct.* **2012**, *102–103*, 64–75.
16. Lignola, G.P.; Prota, A.; Manfredi, G.; Cosenza, E. Performance of FRP confinement on non circular members. In Proceedings of The 3rd fib Congress 2010, Washington, DC, USA, 29 May–2 June 2010.
17. Goodman, R.E. *Introduction to Rock Mechanics*; John Wiley & Sons: Hoboken, NJ, USA, 1989.
18. Li, Y.; Lin, C.; Sung, Y. A Constitute model for concrete confined with carbon fibre reinforced plastics. *Mech. Mater.* **2003**, *35*, 603–619.
19. Teng, J.G.; Huang, Y.L.; Lam, L.; Ye, L.P. Theoretical model for fiber reinforced polymer-confined concrete. *ASCE J. Compos. Constr.* **2007**, *11*, 201–210.
20. Moran, D.A.; Pantelides, C.P. Elliptical and circular FRP-confined concrete sections: A Mohr–Coulomb analytical model. *Int. J. Solids Struct.* **2012**, *49*, 881–898.
21. Girgin, Z.C. Modified johnston failure criterion from rock mechanics to predict the ultimate strength of fiber reinforced polymer (FRP) confined columns. *Polymers* **2014**, *6*, 59–75.
22. Lignola, G.P.; Nardone, F.; Prota, A.; de Luca, A.; Nanni, A. Analysis of RC hollow columns strengthened with GFRP. *ASCE J. Compos. Constr.* **2011**, *15*, 545–556.
23. Campione, G. Influence of FRP wrapping techniques on the compressive behaviour of concrete prisms. *Cem. Concr. Compos.* **2006**, *28*, 497–505.

24. Rousakis, T.C.; Karabinis, A.I.; Kiousis, P.D. FRP-confined concrete members: Axial compression experiments and plasticity modelling. *Eng. Struct.* **2007**, *29*, 1343–1353.
25. Wang, L.M.; Wu, Y.F. Effect of corner radius on the performance of CFRP-confined square concrete columns: Test. *Eng. Struct.* **2008**, *30*, 493–505.
26. Harries, K.A.; Carey, S.A. Shape and "gap" effects on the behaviour of variably confined concrete. *Cem. Concr. Res.* **2003**, *33*, 881–890.
27. Shehata, I.A.E.M.; Carneinro, L.A.V.; Shehata, L.C.D. Strength of short concrete columns confined with CFRP sheet. *Mater. Struct.* **2002**, *35*, 50–58.
28. Lam, L.; Teng, J.G.; Cheung, C.H.; Xiao, Y. FRP-confined concrete under cyclic axial compression. *Cem. Concr. Compos.* **2006**, *28*, 949–958.
29. Ilki, A.; Kumbasar, N. Compressive behaviour of carbon fibre and non-circular cross-sections. *J. Earthq. Eng.* **2003**, *7*, 381–406.
30. Al-Salloum, Y.A. Influence of edge sharpness on the strength of square concrete columns confined with FRP composite laminates. *Compos. B Eng.* **2006**, *38*, 640–650.
31. Harajli, M.H. Axial stress-strain relationship for FRP confined circular and rectangular concrete columns. *Cem. Concr. Compos.* **2006**, *28*, 938–948.
32. Masia, M.J.; Gale, T.N.; Shrive, N.G. Size effects in axially loaded square section concrete prisms strengthened using carbon fiber reinforced polymer wrapping. *Can. J. Civil. Eng.* **2004**, *31*, 1–13.
33. Mandal, S.; Hoskin, A.; Fam, A. Influence of concrete strength on confinement effectiveness of fiber-reinforced polymer jackets. *ACI Struct. J.* **2005**, *102*, 383–392.
34. Tao, Z.; Yu, Q.; Zhong, Y.-Z. Compressive behaviour of CFRP-confined rectangular concrete columns. *Mag. Concr. Res.* **2008**, *60*, 735–745.
35. Micelli, F.; Modarelli, R. Experimental and analytical study on properties affecting the behaviour of FRP-confined concrete. *Compos. B* **2013**, *45*, 1420–1431.
36. Faella, C.; Realfonzo, R.; Salerno, N. Sulla resistenza e deformazione di elementi in c.a. confinati con tessuti in FRP. In Proceedings of the Atti dell'XI Congresso Nazionale "L'ingegneria sismica in Italia", Genova, Italy, 25–29 January 2004 (In Italian).
37. Ombres, L. Influenza del sistema di rinforzo sul confinamento di elementi compressi in calcestruzzo rinforzato con FRP. In Proceedings of the Atti del 16° Congresso C.T.E., Parma, Italy, 9–11 November 2006 (In Italian).
38. Demers, M.; Neale, K.W. Confinement of reinforced concrete columns with fibre-reinforced composite sheets-an experimental study. *Can. J. Civ. Eng.* **1999**, *26*, 226–241.
39. Rochette, P.; Labossiére, P. Axial testing of rectangular column models confined with composites. *J. Compos. Constr.* **2000**, *4*, 129–136.
40. Chaallal, O.; Shahawy, M.; Hassa, M. Performance of axially loaded short rectangular columns strengthened with carbon FRP wrapping. *J. Compos. Constr.* **2003**, *7*, 200–208.
41. Parvin, A.; Wang, W. Behavior of FRP jacketed concrete columns under eccentric loading. *J. Compos. Constr.* **2001**, *5*, 146–152.